Prediction model of PTO shaft fatigue damage considering sandy loam and loam in rotary-tillage operation

Moon-Kyeong Jang,[1,2#] Seung-Jun Kim,[1,2#] Young-Hoo Cho,[3] Ju-Seok Nam[1,2]

[1]Department of Biosystems Engineering, Kangwon National University, Chuncheon, Gangwon-do, Korea
[2]Interdisciplinary Program in Smart Agriculture, Kangwon National University, Chuncheon, Gangwon-do, Korea
[3]Department of Agricultural and Biological Engineering, University of Florida, , Gainesville, FL, USA

[#]*These authors contributed equally to this work.*

Correspondence: Ju-Seok Nam, Department of Biosystems Engineering, Kangwon National University, Chuncheon, Korea.
E-mail: njsg1218@kangwon.ac.kr

Contributions: MKJ, conceived and designed the study, analyzed data, drafted the manuscript, revisions; SJK, conceived and designed the study, analyzed data, drafted the manuscript and contributed to data interpretation; YHC, conducted the investigation, developed the methodology, collected data; JSN, conceptualized the research and handled the writing, review, and editing. All authors approved the final version for publication.

Key words: fatigue damage; prediction model; rotary tillage; soil strength; stress.

Conflict of interest: the authors declare no competing interests, and all confirm accuracy.

Acknowledgments: this work was partly supported by Innovative Human Resource Development for Local Intellectualization program through the Institute of Information & Communications Technology Planning & Evaluation (IITP) grant funded by the Korea government (MSIT) (IITP-2024-RS-2023-00260267, 50) and Korea Institute of Planning and Evaluation for Technology in Food, Agriculture and Forestry (IPET) through Machinery Mechanization Technology Development Program for Field Farming Program, grant funded by Ministry of Agriculture, Food and Rural Affairs (MAFRA) (RS-2023-00235957, 50).

Key words: fatigue damage; prediction model; rotary tillage; soil strength; stress.

Received: 18 October 2024.
Accepted: 20 January 2025.

Journal of Agricultural Engineering 2025; LVI:1610
doi:10.4081/jae.2025.1610

Abstract

In this study, the fatigue damage to a power takeoff (PTO) shaft was evaluated under various operating conditions in rotary-tillage operations, considering soil strength and texture. Pearson correlation analysis was conducted to identify the significant variables influencing PTO shaft fatigue damage, and a prediction formula was derived through regression analysis using these variables. The PTO shaft exhibited increased shear stress with higher transmission gear stages, PTO gear stages, or soil properties, including strength and texture. The fatigue damage increased with higher transmission gear stages and soil strength while decreasing with higher PTO gear stages. Notably, as the PTO gear stage increased, the mean stress increased; however, the stress amplitude and equivalent completely reversed stress significantly reduced fatigue damage. Statistical analyses revealed a strong correlation between PTO shaft fatigue damage and factors such as tractor travel speed, PTO shaft power consumption, PTO shaft rotational speed properties, including strength and texture. The developed prediction equation, incorporating all significant variables, demonstrated, with a coefficient of determination (R^2) of 0.93 and a root mean square error (RMSE) of 2.94×10^{-9}. This equation effectively identifies trends in PTO shaft fatigue damage based on key operational variables. Furthermore, the findings emphasize the critical role of soil texture in assessing PTO shaft fatigue damage.

Introduction

Agricultural tractors are versatile machines capable of performing various tasks, such as tillage, seeding, and harvesting, by attaching appropriate implements (Kim *et al.*, 2023a). Tillage plays a vital role in establishing a soil environment suitable for crop cultivation. However, excessive stress caused by torque on the tractor can result in increased loads and higher energy consumption during operations (Kim *et al.*, 2020a; Hwang *et al.*, 2022a). Tillage operations are typically categorized into primary tillage, which converts soil into large clods, and secondary tillage, which pulverizes the clods into smaller particles using tools such as plows, harrows, and rotavators (Myung and Lee, 2009; Nam *et al.*, 2012). In recent years, there has been a growing trend of completing both primary and secondary tillage simultaneously using a single rotavator. This approach has been adopted to reduce working hours and labor demands (Kim *et al.*, 2013a; Kim *et al.*, 2013b; Hensh *et al.*, 2021; Al-Dosary *et al.*, 2022). The rotavator is mounted on the tractor's three-point hitch, and tillage is per-

formed by receiving rotational power from the power takeoff (PTO) shaft. Rotary tillage using a rotavator requires a relatively higher working load and power compared to traditional methods like plowing and harrowing (Libin *et al.*, 2010; Yadav *et al.*, 2017). Furthermore, improper operating conditions, such as incorrect gear selection incompatible with soil characteristics, can significantly reduce the efficiency of tillage operations due to excessive loads (Kumari and Raheman, 2023). During rotary tillage, the stress exerted on the tractor is influenced by factors such as transmission gear stages, PTO gear stages, and soil properties (Naderloo *et al.*, 2009; Lee *et al.*, 2015; Kim *et al.*, 2020b). These load characteristics are primarily evaluated using metrics like engine and PTO shaft torque, consumed power, and the fatigue life of the PTO shaft (Baek *et al.*, 2019; Kim *et al.*, 2020c). As most of the operational power is transmitted through the PTO shaft, conducting a detailed load analysis is essential to ensure the safety and efficiency of rotary-tillage operations (Kim *et al.*, 2020c; Kumari and Raheman, 2023). Consequently, several studies have analyzed the loads acting on PTO shafts. For instance, Baek *et al.* (2019) investigated engine torque characteristics during rotary tillage using a 78-kW class tractor. The study categorized the entire operation into tillage and headland turning sections, revealing that equivalent torque was higher during tillage than during headland turning. The authors emphasized the importance of incorporating the torque profile generated during actual agricultural work for the optimal design of tractor engines. Kim *et al.* (2020c) analyzed engine load variations based on torque, considering transmission and PTO gear stages during rotary tillage, plow tillage, and potato harvesting using a 24-kW class tractor. Their findings indicated that engine load followed the order of rotary tillage, plow tillage, and harvesting. Additionally, engine load increased with higher transmission and PTO gear stages. Kim *et al.* (2018) investigated the torque and fatigue life of PTO shafts during rotary tillage using a 30-kW class tractor. The study revealed that fatigue life decreased as the PTO gear stage increased. Similarly, Kim *et al.* (2019) examined torque and fatigue life in a rotary-tillage operation using a 78-kW class tractor, finding that a lower PTO gear stage and a higher transmission gear stage were associated with reduced fatigue life. These contrasting trends in fatigue life across PTO gear stages highlight the need for further experiments to build a comprehensive database. Kim *et al.* (2023b) analyzed stress and torque during rotary tillage with a 42-kW class tractor in both primary-tilled and untilled soils. Their results confirmed that torque and consumed power were lower in primary-tilled soil compared to untilled soil, and both increased with higher transmission gear stages. Similarly, Ryu *et al.* (2012) investigated engine and PTO shaft torque and power consumption in a 75-kW class tractor. Their findings indicated that power consumption and PTO shaft torque increased with higher transmission gear stages and lower PTO gear stages.

Existing studies have predominantly analyzed torque and stress characteristics during rotary tillage, focusing on trends based on transmission and PTO gear stages. These studies primarily evaluated engine and PTO shaft torque to assess load characteristics and fatigue life. However, soil strength is another critical variable that significantly influences torque and stress during tillage operations (Kumar *et al.*, 2012; Mallarino and Wittry, 2004). Even under identical transmission and PTO gear stages, variations in soil strength can result in differing degrees of PTO shaft fatigue damage. This study analyzed the effects of soil strength, operating location, and transmission and PTO gear stages on the stress caused by torque acting on PTO shafts during rotary-tillage operations. The primary objective was to develop a prediction equation for PTO shaft fatigue damage by statistically evaluating the effects of major operating variables. The findings of this study provide fundamental data for the fatigue design of PTO shafts, offering valuable insights for improving the reliability and efficiency of rotary-tillage operations.

Materials and Methods

Tractor and rotavator

The rotary-tillage operation was conducted using a rotavator attached to a 42-kW class tractor to measure torque. The shape and specifications of the tractor are presented in Figure 1 and Table 1. The transmission system of the tractor consisted of four main gears and six subgears, with nominal travel speeds determined by their combinations. The PTO gear system included three gears, with

Figure 1. Shape of the tractor used.

Table 1. Specifications of the tractor used.

Item		Specification
Nation / Company / Model		Korea / TYM / TX58
Engine rated power (kW)		42
PTO rated power (kW)		39
Weight (kg)		3,894
Transmission	No. of main gears	4 (1, 2, 3, 4)
	No. of sub gears	6 (L, M, H & Ultra-low speed On/Off)
No. of PTO gears	3 (1, 2, 3)	
Tire size	Front	11.2-20
	Rear	14.9-30

rated rotational speeds of 540, 720, and 1,000 rpm for each gear, respectively. For the rotavator, a product within the applicable power range was selected, considering that the rated power of the tractor PTO shaft was 39 kW. The shape and specifications of the rotavator are detailed in Figure 2 and Table 2.

Measurement system

The data acquisition system (DAQ) was based on Dewesoft X (Dewesoft 3X, Dewesoft, Trbovlje, Slovenia). During the rotary-tillage operation, the system measured the tractor's actual travel speed, as well as the torque and rotational speed of the engine and PTO shaft (Figure 3). The actual travel speed of the tractor was recorded using an RTK-GPS installed inside the cabin. The shape and specifications of the RTK-GPS are presented in Figure 4 and Table 3. The torque and rotational speed of the engine and PTO shaft were measured using a flanged torque transducer and a proximity sensor. The data sampling rate was set to 1 kHz in accordance with the torque transducer's specifications. The shape and specifications of the torque transducer and proximity sensor are shown in Figure 5 and Tables 4 and 5, respectively.

The power consumed by the engine and the PTO shaft was calculated using the measured torque and rotational speed, as represented in Eq. 1 and Eq. 2, respectively:

$$P_e = \frac{2\pi \times T_e \times N_e}{60{,}000} \quad \text{(Eq. 1)}$$

where: P_e = consumed power of engine (kW); T_e = torque of engine shaft (N·m); N_e = rotational speed of engine shaft (rpm)

$$P_{PTO} = \frac{2\pi \times T_{PTO} \times N_{PTO}}{60{,}000} \quad \text{(Eq. 2)}$$

where: P_{PT0} = consumed power of PTO shaft (kW); T_{PT0} = PTO shaft torque (N·m); N_{PT0} = rotational speed of PTO shaft (rpm).

Operating conditions

Measurements were conducted under various tillage operating conditions to analyze stress due to torque (Figure 6). The typical travel speed for rotary-tillage operations with medium-sized tractors generally ranges from 1.5 to 3.5 km h^{-1} (Kim *et al.*, 2019; Kim *et al.*, 2018; Ryu *et al.*, 2013). Accordingly, the transmission gear stages were selected as the 2nd to 4th stages of the main gears and the L (ultra-low-speed off) stage of the sub-gear (Table 6). For PTO gear stages, only the 1st and 2nd stages -commonly employed in rotary-tillage operations- were applied. The 3rd stage was excluded due to its potential to exert excessive loads on the PTO shaft, making normal operation infeasible (Kim *et al.*, 2018; Ryu *et al.*, 2013).

Figure 2. Shape of the tractor used.

Figure 3. DAQ system for measurement.

Figure 4. Shape of the RTK-GPS used.

Table 2. Specifications of the rotavator used.

Item	Specification
Model	WJ185A
Nation / Company	Korea / Woongjin
No. of flanges	7
No. of blades for each flange	6
Rated power (kW)	36-41
Tillage width (mm)	2,020
Tillage depth (mm)	120

Tillage pitch, defined as the length of soil tilled in the forward direction during one complete rotation of the rotavator blade, depends on the tractor's travel speed and the PTO shaft's rotational speed. Tillage pitch influences both tillage performance and the load on the PTO shaft, with smaller tillage pitches corresponding to higher soil pulverization ratios (Kim *et al.*, 2018; Park *et al.*, 2002). The tillage pitch was calculated using Eq. 3, and its impact on PTO shaft fatigue damage was analyzed in this study (Kim *et al.*, 1997). The tillage pitches used in the analysis are presented in Table 7.

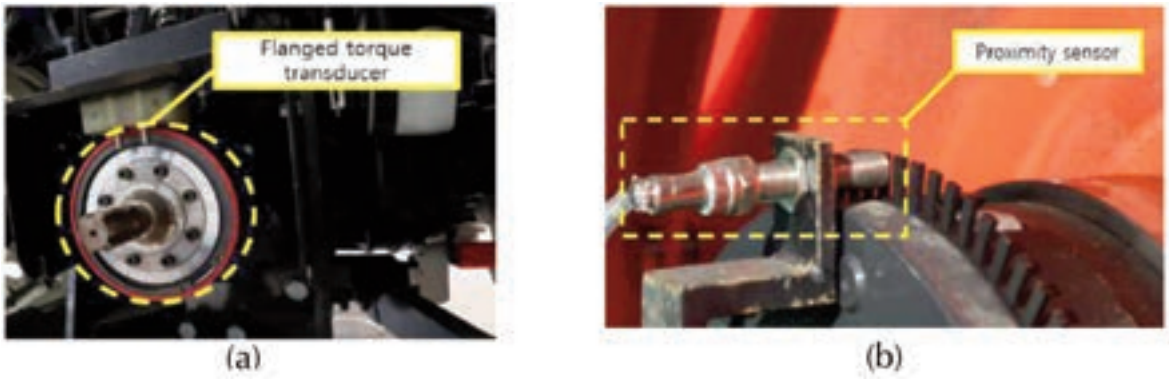

Figure 5. Torque and rotational speed measuring equipment. **a**) Flanged torque transducer; **b**) Proximity sensor.

Table 3. Specifications of the RTK-GPS used.

Item	Specification	
Model		Duro Inertial
Nation / Company		USA / Swift Navigation
Length × Width × Height (mm)		130 × 130 × 65
Weight (Kg)		0.8
RTK accuracy	Horizontal Vertical	0.01 m + 1 ppm 0.015 m + 1 ppm
IMU sampling rate (Hz)	100	
GPS sampling rate (Hz)	10	

Table 4. Specifications of the flanged torque transducer used.

Item	Specification
Model	PCM 16
Nation / Company	Germany / MANNER
Supply voltage (V)	5
Maximum measuring torque (kN·m)	15
Maximum sampling rate (kHz)	1

Table 5. Specifications of the proximity sensor used.

Item	Specification
Model	CYGTS211B-PO2
Nation / Company	Germany / Chen Yang Technologies GmbH & Co. KG
Diameter / Screw size (mm)	M12×1 / M16×1
Sensing distance (mm)	< 3
Sensing object	Ferrous metal targets

Table 6. Travel speeds used for each transmission gear stages in this study.

Transmission gear		Travel speed (km h^{-1})
Sub gear	Main gear	
L (Ultra low speed off)	2	1.57
	3	2.25
	4	3.00

$$p = \frac{60 \times V_{act}}{Z \times N_{PTO}} \quad \text{(Eq. 3)}$$

where: p = tillage pitch (cm); V_{act} = actual travel speed of tractor (cm s^{-1}); Z = number of rotavator blades for each flange; N_{PTO} = rotational speed of PTO shaft (rpm).

Field tests were conducted on two distinct soil types in Sinbuk-eup, Chuncheon-si, Gangwon-do, South Korea (Figure 7). Rotary-tillage operations were performed within rectangular working areas at each site, with variations in operating conditions (Figure 8). In Figure 8, the operating conditions are represented by the transmission and PTO gear stages, where «L2P1» indicates transmission gear stage L2 (sub-gear L and main gear 2) and PTO gear stage 1. The number following the hyphen denotes the test repetition. Each operating condition was tested three times under identical settings. Even within the same field, soil properties can exhibit significant non-uniformity, varying by location. This necessitates location-specific sampling to ensure accurate soil characterization (Mallarino and Wittry, 2004; Kerry and Oliver, 2004). Among soil properties, soil strength is a critical variable influencing the stress experienced during tillage operations, making its measurement and analysis essential at each operating location (Kim *et al.*, 2020a; Kumar *et al.*, 2012). Soil sampling was conducted by dividing the test area into evenly spaced grids and extracting samples from each grid intersection (Wollenhaupt and Wlkowski, 1994; Asare and Segarra, 2018). In this study, soil strength at each intersection was

Figure 7. Location and shape of experimental sites.

Figure 6. Tillage operation of tractor with rotavator attached.

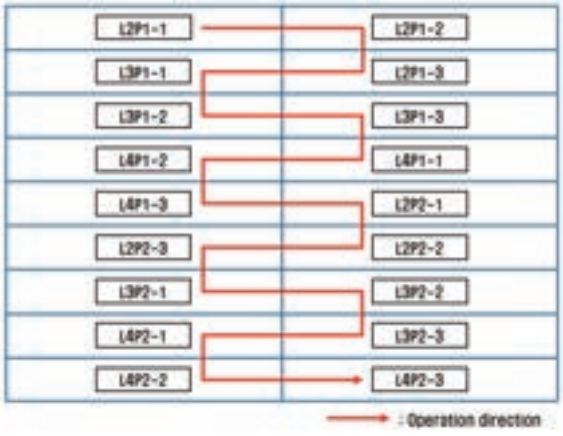

Figure 8. Operating conditions for each experimental site.

Table 7. Tillage pitches used in this study.

Operating conditions		Tillage pitch (cm)
Site 1	L2P1	0.82
	L3P1	1.18
	L4P1	1.57
	L2P2	0.62
	L3P2	0.89
	L4P2	1.19
Site 2	L2P1	0.83
	L3P1	1.20
	L4P1	1.61
	L2P2	0.63
	L3P2	0.90
	L4P2	1.21

measured by dividing the test field into a square grid with dimensions of 3 × 3 m, as shown in Figure 9. Additional measurements were taken for soil texture and water content (Tan, 2005). The cone index (CI) was used as a representative value for soil strength, measured following the standard test method specified by the American Society of Agricultural and Biological Engineers (ASABE) using a standard soil cone penetrometer (DIK-5532, Daiki, Saitama, Japan) (Jabro *et al.*, 2021; ASABE, 2018; ASABE, 2019). The specifications of the soil cone penetrometer are presented in Table 8. Considering that the typical tillage depth of a rotavator ranges between 100 and 200 mm and that the rotavator used in this study had a tillage depth of 120 mm, CI measurements were taken at 10-mm intervals up to a depth of 200 mm from the soil surface (Kim *et al.*, 2013a). Figure 8 displays 18 sections for each operating condition, comprising two horizontal and nine vertical sections, while Figure 9 illustrates the grid layout with 135 intersections, including 15 horizontal and nine vertical intersections. To align the operating conditions with the soil strength at each location, the experimental design incorporated seven or eight soil strength measurement points for each operating condition (Figure 10). This design enabled simultaneous consideration of the effects of soil strength, transmission gear stages, and PTO gear stages on the stress experienced by the PTO shaft. Soil sampling for texture and water content measurements was conducted using soil collection tubes (DIK-1801; Daiki Rika Kogyo Co., Ltd., Akagidai, Japan) and related devices (DIK-1815; Daiki Rika Kogyo Co., Ltd.). Soil water content was calculated using Eq. 4, based on the weight of the soil sample before and after drying for 24 hat 110°C in an oven:

$$W = \frac{100 \times (W_s - W_{dry})}{W_s} \quad \text{(Eq. 4)}$$

where: W = soil water content (%); W_{dry} = weight of drying soil (g); W_s = weight of soil sample before drying (g).

Soil texture was classified using the USDA (United States Department of Agriculture) soil classification triangle, which is based on soil particle size distribution determined using standard sieves.

Derivation of the fatigue damage of the PTO shaft

Fatigue failure is a phenomenon in which mechanical components fail due to the propagation of small cracks caused by repetitive loading. During rotary-tillage operations, the load generated produces torque on the PTO shaft, leading to fatigue failure through repeated torque application. The fatigue life of the PTO shaft is defined as the time until fatigue failure occurs and can be determined through fatigue damage analysis (Kamal and Rahman, 2018; Santecchia *et al.*, 2016). In this study, the fatigue damage of

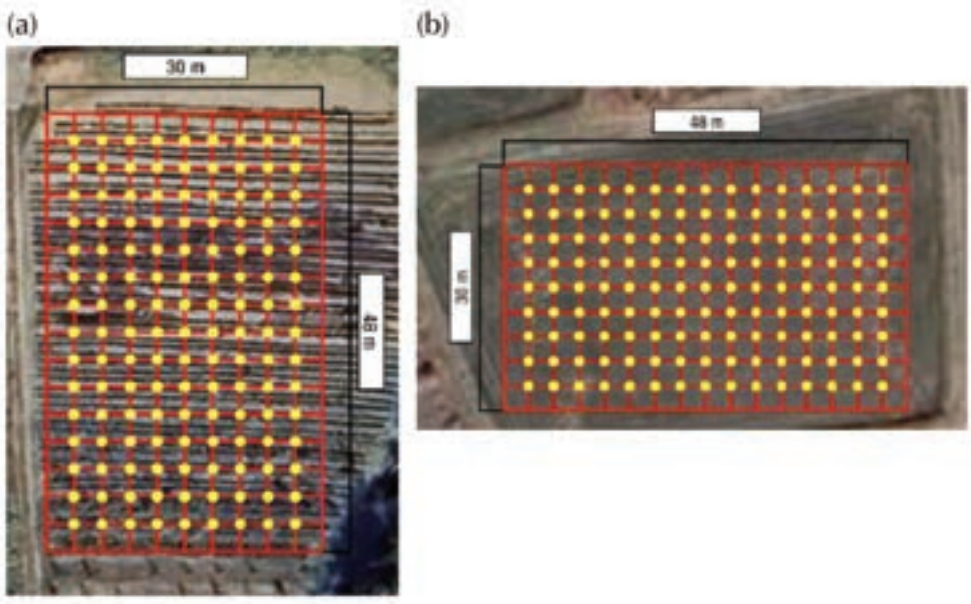

Figure 9. Grid method for soil sampling.

Table 8. Specifications of the soil cone penetrometer used.

Item	Specification
Model	DIK-5532
Nation / Company	Japan / Daiki
Length × Width × Height (mm)	345 × 212 × 144
Weight (kg)	4
Measuring range (kPa)	179-4,903
Measuring depth (mm)	300-600

the PTO shaft was computed using fatigue analysis software (nCode GlyphWorks 2019, HBM, UK) with the measured PTO shaft torque data (Figure 11).

The PTO shaft, which transmits rotational power, experiences torque and shear stress due to torsion. These factors are critical in fatigue damage analysis. To calculate fatigue damage from the torque data, Eq. 5 was used to convert the measured PTO shaft torque into shear stress:

$$\tau_{PTO} = \frac{16 \times T_{PTO}}{\pi \times (d_{PTO})^3} \quad \text{(Eq. 5)}$$

where: τ_{PT0} = maximum shear stress of PTO shaft (Pa); T_{PT0} = PTO shaft torque (N·m); d_{PT0} = pitch diameter of PTO shaft (m).

The torque experienced by the PTO shaft during rotary-tillage operations exhibits significant fluctuations and non-periodic characteristics (Kim *et al.*, 2023b). To calculate fatigue damage from these non-periodic loads, both the amplitude and occurrence frequency of the loads must be derived (Grubisic, 1994). In this study, rainflow counting was employed to quantify the amplitude and frequency of shear stress. Rainflow counting is a method used to count strain hysteresis loops in a strain-time diagram. The process involves rotating the local maximum point of the load data to the right, the local minimum point to the left, and simulating a virtual raindrop falling downward from each local maximum and minimum point. The load amplitude, corresponding to the difference between the starting and ending points of the raindrop, is counted as a half-cycle (Anthes, 1997). Rainflow counting is used in various industries because of its applicability to highly variable and complex loads (Amzallag *et al.*, 1994). Applying rainflow counting to the shear stress data derived using Eq. 5 facilitated the extraction of information on the mean and amplitude of the shear stress and its respective occurrence frequency. The material characteristics widely used to derive the fatigue damage and fatigue life of mechanical components are the S-N curves. This curve illustrates the number of loading cycles (life cycles) leading to fatigue failure for each magnitude of completely reversed stress, with a mean of zero (Kim *et al.*, 2011). The material for the PTO shaft was SCM420h, a chromium-molybdenum alloy steel, with its mechanical properties listed in Table 9 (Natpukkana *et al.*, 2018; Lee *et al.*, 2004). The S-N curve of the steel can be determined from the fatigue strengths at 103 and 106 cycles, and factors such as the type of load, material size, surface treatment, operating temperature, and reliability should be considered. The fatigue strengths at 103 and 106 cycles were computed using Eq. 6 and Eq. 7, with the coefficient values specified in Table 10. The load and reliability factors were established by selecting torsion as the load type and a 90% reliability level, respectively. The gradient, surface, and temperature factors were determined considering the diameter of the PTO shaft, material processing method, and operating temperature (Shigley *et al.*, 2020). The resulting S-N curve for the PTO shaft material is shown in Figure 12.

$$S_f = 0.9 S_{us} C_T \quad \text{(Eq. 6)}$$

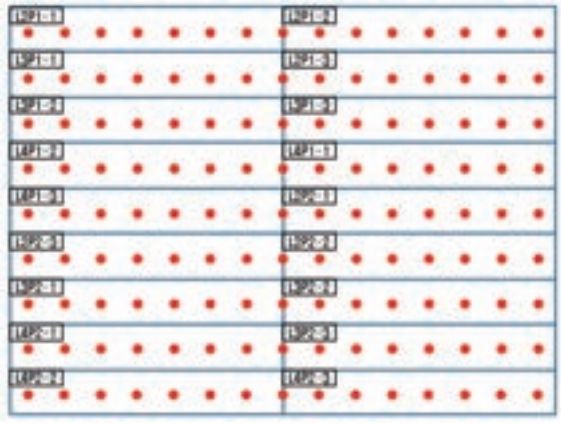

Figure 10. Matching operation conditions and grid sampling spots.

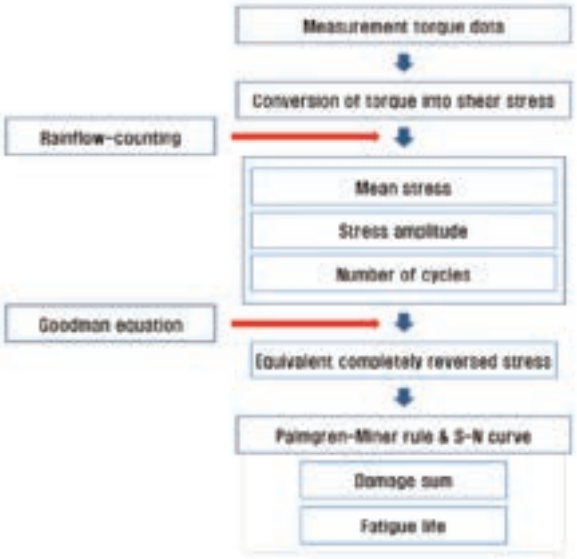

Figure 11. Matching operation conditions and grid sampling spots.

Table 9. Specifications of SCM420h.

Item	Specification
Material	SCM420h
Yield strength (MPa)	380
Poisson's ratio	0.3
Ultimate tensile strength (MPa)	790
Elastic Modulus (GPa)	211
Ultimate shear strength (MPa)	632
Shear Modulus (GPa)	81.15

$$S_n = 0.5 S_{ut} C_L C_G C_S C_T C_R \quad \text{(Eq. 7)}$$

where: S_f = fatigue strength for 10^3 cycles (MPa); S_n = fatigue strength for 10^6 cycles (MPa); S_{us} = ultimate shear strength of the material (MPa); S_{ut} = ultimate tensile strength of the material (MPa); C_L = load factor; C_G = gradient factor; C_S = surface factor; C_T = temperature factor; C_R = reliability factor. To calculate fatigue damage and life using the S-N curve, the stress encompassing both the mean and amplitude was converted into an equivalent completely reversed stress using the Goodman equation (Eq. 8):

$$\tau_{eq} = \frac{S_{us} \times \tau_a}{S_{us} - \tau_m} \quad \text{(Eq. 8)}$$

where: τ_{eq} = equivalent completely reversed shear stress (MPa); S_{us} = ultimate shear strength of the material (MPa); τ_a = shear stress amplitude (MPa); τ_m = mean shear stress (MPa). By substituting the equivalent completely reversed stress into the S-N curve, the life cycle at which fatigue failure occurs can be determined. The fatigue damage was then calculated using the Palmgren–Miner linear cumulative damage rule (Eq. 9). This rule calculates total fatigue damage by summing the partial damage caused by all applied stresses, assuming fatigue failure occurs when total fatigue damage equals 1.0 (Lee and Lee, 1998). The fatigue life was subsequently derived using the total fatigue damage, as shown in Eq. 10:

$$D_t = \sum_{i=1}^{k} \frac{n_i}{N_i} \quad \text{(Eq. 9)}$$

where: Dt = total fatigue damage; ni = Number of actually applied cycles for ith stress; Ni = life cycles for ith stress;

$$L_f = \frac{1}{D_t} \times t \quad \text{(Eq. 10)}$$

where: L_f = fatigue life; D_t = total fatigue damage; t = working time that generates the total fatigue damage.

Development of PTO shaft fatigue damage prediction formula

The fatigue damage of the PTO shaft was assessed using 30 sec of working data for each operating condition. A prediction formula for fatigue damage was developed through statistical analysis. The stress induced by torque during rotary-tillage operations is influenced by factors such as transmission and PTO gear stages, as well as soil properties. Additionally, tractor travel speed, consumed power of the engine and PTO shaft, rotational speed of the PTO shaft, and tillage pitch vary depending on the transmission and PTO gear stages. Therefore, the operating variables affecting PTO shaft fatigue damage were identified as tractor travel speed, rotational speed of the PTO shaft, consumed power of the engine and PTO shaft, tillage pitch, and soil strength. Pearson's correlation analysis was conducted to examine the relationships between PTO shaft fatigue damage and the identified operating variables. Subsequently, regression analysis was performed to develop a prediction equation. Variables showing a significant correlation were used as independent variables, while PTO shaft fatigue damage was set as the dependent variable. Methods for selecting variables for the prediction equation include forward selection, backward elimination, and the stepwise method (Blanchet *et al.*, 2008; Sutter and Kalivas, 1993; Thompson, 1995). The stepwise method, employed in this study, alternates between forward selection and backward elimination. Independent variables are added as in forward selection, with the F-statistic significance level assessed when a second variable is introduced. Variables are retained if they satisfy the F-statistic significance level; otherwise, they are removed. This process continues until no further additions or removals of variables are possible. The accuracy of the developed prediction equation was evaluated using the coefficient of determination (R^2) and the root mean square error (RMSE) as shown in Eqs. 11 and 12, respectively. R^2 represents the proportion of variance in the predicted values relative to the measured values, expressed as a percentage. Values closer to 1.0 indicate higher accuracy of the regression model (Rousson and Gosoniu, 2007; Hwang *et al.*, 2022b). RMSE quantifies the error between measured and predicted values; smaller RMSE values indicate greater prediction accuracy (Karunasingha, 2022; Chai and Draxler, 2014; Hodson, 2022).

$$R^2 = 1 - \frac{\sum_{i=1}^{n} (y_i - \hat{y}_i)^2}{\sum_{i=1}^{n} (y_i - \bar{y})^2} \quad \text{(Eq. 11)}$$

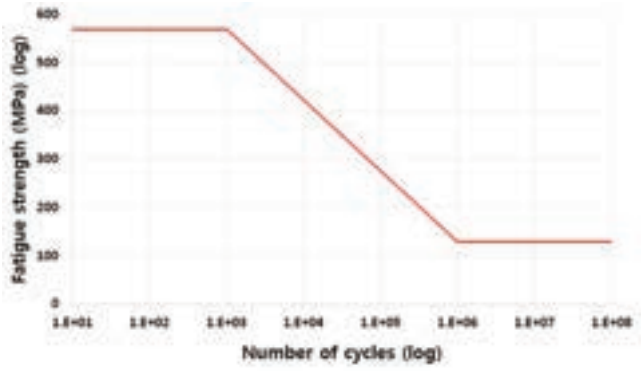

Figure 12. S-N curve of SCM420h for shear stress.

Table 10. Values of each parameter for fatigue strength.

Parameters	Values
Load factor (C_L)	0.58
Gradient factor (C_G)	0.85
Surface factor (C_S)	0.77
Temperature factor (C_T)	1.0
Reliability factor (C_R)	0.897

$$RMSE = \sqrt{\frac{1}{n} \times \sum_{i=1}^{n} (y_i - \hat{y}_i)^2} \quad \text{(Eq. 12)}$$

where: y_i =actual values; $\hat{y}_i$ = predicted values; $\bar{y}$ = average of values.

Results and Discussions

Soil properties of test sites

Table 11 presents the measurement results for soil texture and water content at each test site. The average values at the grid intersections of each site were used as representative values. At Site 1, the sand, silt, and clay contents were 46.0%, 34.0%, and 20.0%, respectively, classifying the soil as loam. Site 2 exhibited 62.0% sand, 24.0% silt, and 14.0% clay, classifying the soil as sandy loam. The average water content for Sites 1 and 2 was 20.6% and 21.4%, respectively, indicating similar moisture levels between the two fields. The soil strength at each site was determined as the average value within 50 mm intervals and the overall average value for the entire depth range of 0–200 mm, as shown in Table 12. At both sites, soil strength increased with depth from the soil surface. The average soil strength within the 0–200 mm depth range was 1,087 kPa at Site 1 and 1,316 kPa at Site 2, indicating that Site 2 exhibited relatively higher soil strength. Table 13 displays the results of correlating the operating conditions with the average soil strength, using the total average value within the 0–200 mm depth range as the representative soil strength. The observed variability in soil strength across different operating locations, even within the same site, highlights the importance of conducting a load analysis that accounts for deviations in soil strength.

PTO shaft fatigue damage

Figure 13 illustrates the shear stress profile of the PTO shaft. The shear stress values, averaged over the measured time domain, exhibited an upward trend with increasing transmission and PTO

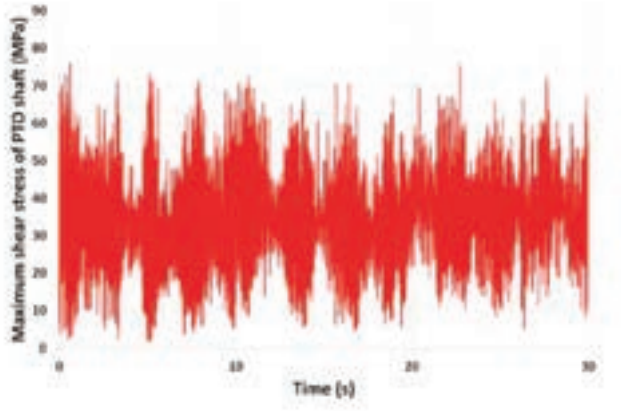

Figure 13. Measured maximum shear stress of PTO shaft.

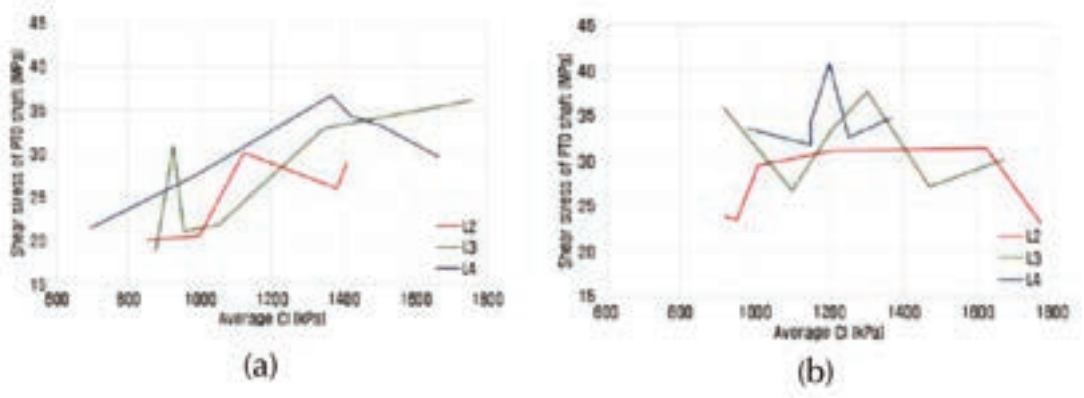

Figure 14. Shear stress of PTO shaft according to average CI. **a**) PTO gear 1; **b**) PTO gear 2.

Table 11. Soil texture and water contents of test sites.

Sites	Sand (%)	Silt (%)	Clay (%)	Soil texture	Water contents (%)
Site 1	46.0	34.0	20.0	Loam	20.6
Site 2	62.0	24.0	14.0	Sandy loam	21.4

Table 12. Soil strength of test sites.

Items	Depth (mm) 0-50	50-100	100-150	150-200	Average (0-200)
CI (kPa)					
Site 1	482	857	1,332	1,676	1,087
Site 2	607	1,213	1,585	1,856	1,316

gear stages. Figure 14 categorizes the shear stress by soil strength for the same transmission and PTO gear stages. In the 1st PTO gear stage, shear stress increased as the overall soil strength increased. However, in the 2nd PTO gear stage, no distinct trend was observed with respect to soil strength. Shear stress data in the time domain were converted into frequency-domain data using the rainflow counting method. Figure 15 presents the mean stress and stress amplitude derived from rainflow counting, along with the equivalent completely reversed stress calculated using the Goodman equation. The mean stress exhibited an increasing trend with higher transmission and PTO gear stages. Interestingly, the stress amplitude and equivalent completely reversed stress decreased with increasing PTO gear stages, showing minimal influence from the transmission gear stage. This suggests that the equivalent completely reversed stress is more influenced by the stress amplitude than by the mean stress, as evidenced by their

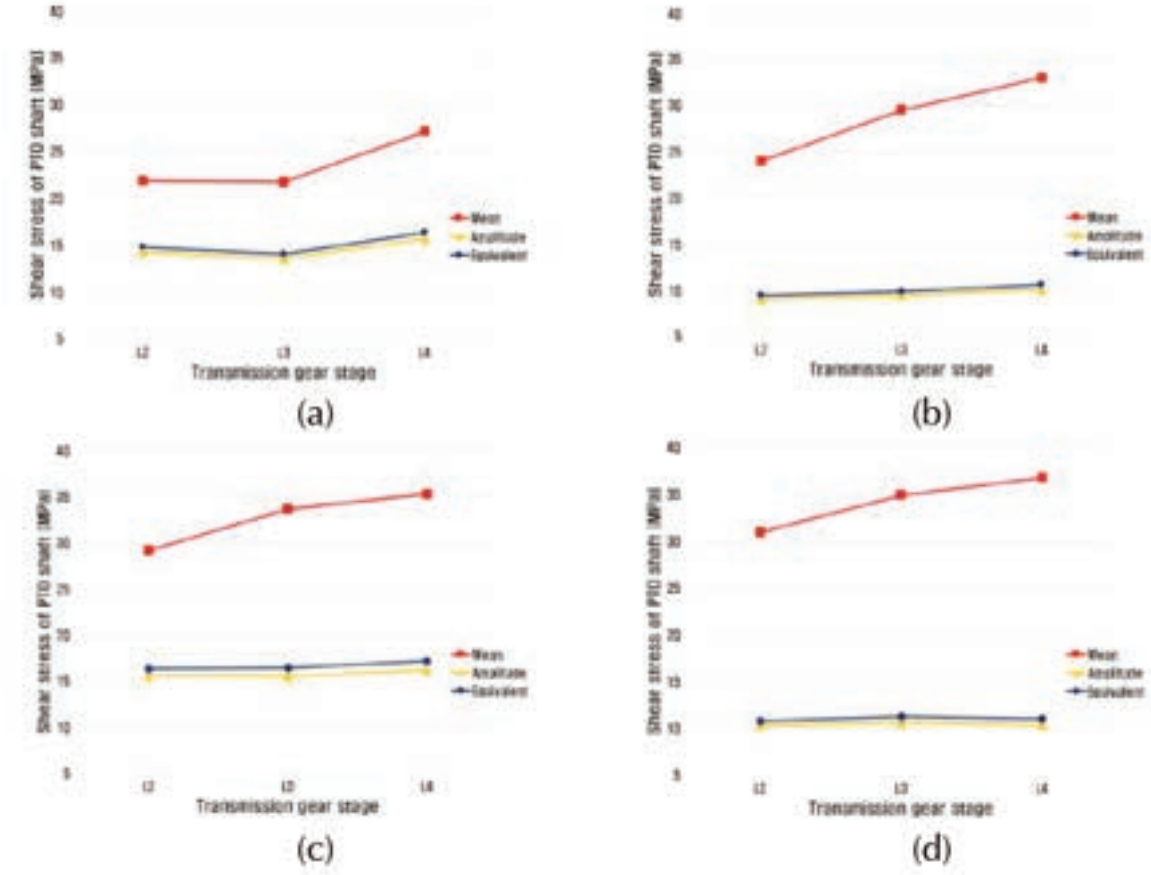

Figure 15. Frequency based mean, amplitude, and equivalent completely revered shear stress according to transmission and PTO gear stages. **a**) Site 1 – PTO gear 1; **b**) Site 1 – PTO gear 2; **c**) Site 2 – PTO gear 1; **d**) Site 2 – PTO gear 2.

Table 13. Soil strength according to operating locations.

Operating conditions		Average CI (kPa)		
		1	2	3
Site 1	L2P1	993	1,003	855
	L3P1	955	1,051	876
	L4P1	695	1,663	989
	L2P2	921	1,768	953
	L3P2	1,206	1,101	1,471
	L4P2	982	1,253	1,151
Site 2	L2P1	1,121	1,380	1,411
	L3P1	1,344	1,761	927
	L4P1	1,504	1,421	1,365
	L2P2	1,209	1,010	1,623
	L3P2	917	1,302	1,669
	L4P2	1,201	1,152	1,369

similar magnitudes and trends. Additionally, even under identical operating conditions, deviations in stress were observed due to variations in soil strength at different operating locations. A consistent increase in stress was observed with higher soil strength. Figure 16 categorizes the equivalent completely reversed stress by soil strength for the same transmission and PTO gear stages. Table 14 provides the frequency percentage for each section by categorizing the equivalent completely reversed stress into 5 MPa intervals based on the operating conditions. Figures 17 and 18 demonstrate that as the transmission gear stage increased and the PTO

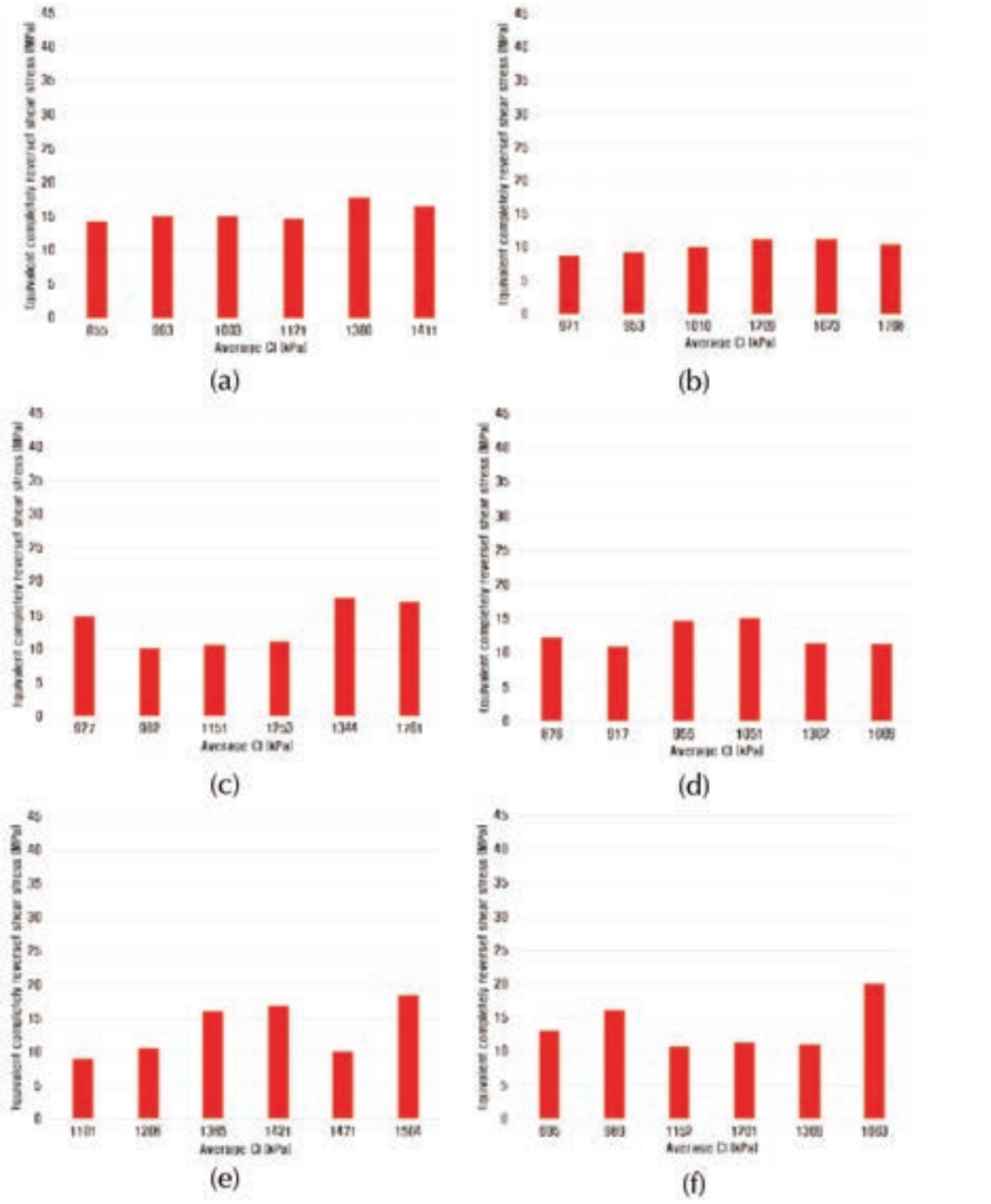

Figure 16. Equivalent completely reversed shear stress according to average CI. **a**) L2P1; **b**) L2P2; **c**) L3P1; **d**) L3P2; **e**) L4P1; **f**) L4P2.

gear stage decreased, the frequency of larger equivalent completely reversed stresses tended to rise. Since the equivalent completely reversed stress directly affects fatigue life, higher transmission gear stages and lower PTO gear stages resulted in shorter fatigue life for the PTO shaft. Figure 19 illustrates the percentage frequency of equivalent completely reversed stresses of 20 MPa or more based on soil strength under the same transmission and PTO gear stages. Generally, the frequency of larger equivalent completely reversed stresses increased with higher soil strength, indicating that operating in high-strength soil reduced the PTO shaft's fatigue life. Table 15 presents the fatigue damage of the PTO shaft under various operating conditions. Using the L2P2 condition of Site 1, where the lowest fatigue damage occurred, as a reference, the relative fatigue damage under other conditions was quantified as the relative severeness. Figure 20 shows the trends in relative severeness based on transmission and PTO gear stages. The relative severeness increased with higher transmission gear stages and lower PTO gear stages. Furthermore, under different soil conditions, the relative severeness at Site 2 -characterized by higher soil strength- was greater than that at Site 1. This difference is attributed to the higher frequency of large, equivalent, completely reversed stresses under conditions of high transmission gear stages, higher soil strength, and lower PTO gear stages. To improve the safety of the PTO shaft against fatigue failure, rotary-tillage operations with lower transmission gear stages and higher PTO gear stages are recommended. Figure 21 illustrates the relationship between relative severeness and tillage pitch, showing that relative severeness increased with higher tillage pitch values.

Development of PTO shaft fatigue damage prediction formula

Table 16 presents the results of the Pearson correlation analysis, which examined the relationship between PTO shaft fatigue damage and various factors, including tractor travel speed, rotational speed of the PTO shaft, consumed power of the engine and

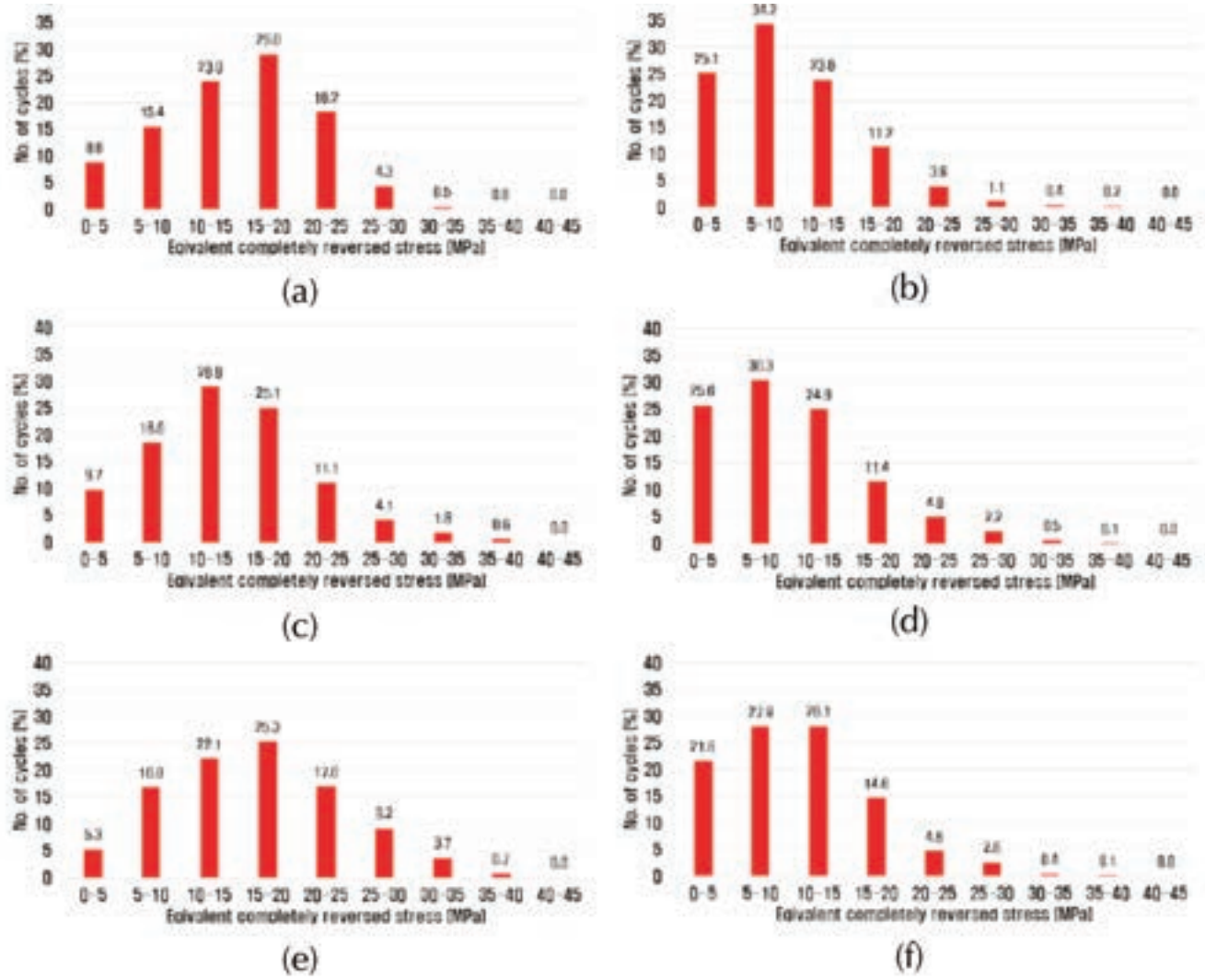

Figure 17. Percentage of equivalent completely reversed shear stress according to operating conditions at site 1. **a**) L2P1; **b**) L2P2; **c**) L3P1; **d**) L3P2; **e**) L4P1; **f**) L4P2.

Table 14. Percentage of actually applied cycles for each equivalent completely reversed shear stress range.

Operating conditions			Percentage of stress cycles (%)								
			0-5	5-10	10-15	15-20	20-25	25-30	30-35	35-40	40-45
Site 1	L2P1	1	8.6	14.8	23.2	27.7	20.4	5.2	0.0	0.0	0.0
		2	9.9	14.8	19.0	30.9	20.8	3.8	0.7	0.0	0.0
		3	7.8	16.6	29.4	28.4	13.4	3.8	0.5	0.0	0.0
		Ave.	8.8	15.4	23.9	29.0	18.2	4.3	0.5	0.0	0.0
	L3P1	1	6.3	17.9	29.3	26.6	12.9	4.2	2.1	0.5	0.0
		2	7.4	17.1	28.2	24.2	14.7	5.8	2.4	0.3	0.0
		3	15.3	20.8	29.6	24.5	5.5	2.1	1.1	1.1	0.0
		Ave.	9.7	18.6	28.9	25.1	11.1	4.1	1.8	0.6	0.0
	L4P1	1	8.6	24.2	28.3	25.8	10.1	2.5	0.5	0.0	0.0
		2	1.7	10.6	14.4	18.9	25.0	20.6	8.3	0.6	0.0
		3	5.4	14.6	22.2	31.4	16.8	5.4	2.7	1.6	0.0
		Ave.	5.3	16.8	22.1	25.3	17	9.2	3.7	0.7	0
	L2P2	1	26.4	38.9	21.7	10.0	2.2	0.4	0.3	0.0	0.0
		2	22.4	30.5	24.6	13.4	5.8	1.9	0.7	0.6	0.0
		3	26.4	33.4	25.0	10.2	3.7	0.9	0.3	0.1	0.0
		Ave.	25.1	34.2	23.8	11.2	3.9	1.1	0.4	0.2	0
	L3P2	1	21.8	27.6	28.0	13.3	6.4	2.4	0.4	0.0	0.0
		2	28.4	34.0	23.8	9.8	2.7	1.1	0.2	0.0	0.0
		3	26.8	29.5	22.8	11.2	5.6	3.1	0.9	0.2	0.0
		Ave.	25.6	30.3	24.9	11.4	4.9	2.2	0.5	0.1	0
	L4P2	1	20.9	31.7	29.1	12.2	3.5	2.6	0.0	0.0	0.0
		2	20.4	25.7	27.8	17.0	6.1	1.7	1.3	0.0	0.0
		3	23.8	26.9	26.4	14.5	4.4	3.5	0.0	0.4	0.0
		Ave.	21.6	27.9	28.1	14.6	4.6	2.6	0.4	0.1	0
Site 2	L2P1	1	10.2	20.6	24.0	18.8	15.7	8.2	2.5	0.0	0.0
		2	2.2	9.0	21.6	30.4	23.7	10.9	1.8	0.3	0.0
		3	8.2	11.9	22.5	23.9	19.2	10.4	3.7	0.2	0.0
		Ave.	6.9	13.8	22.7	24.4	19.5	9.8	2.7	0.2	0
	L3P1	1	5.6	11.7	20.5	22.1	21.6	14.9	3.2	0.3	0.0
		2	7.1	15.9	22.0	19.0	16.7	10.3	6.9	2.1	0.0
		3	10.6	17.6	24.5	24.5	14.4	5.3	1.3	1.6	0.3
		Ave.	7.8	15	22.4	21.9	17.5	10.2	3.8	1.3	0.1
	L4P1	1	6.3	9.5	18.9	24.2	18.4	12.6	8.4	1.6	0.0
		2	6.8	15.8	22.1	20.5	17.4	11.6	4.7	1.1	0.0
		3	8.5	16.0	22.3	22.9	16.0	9.0	2.7	2.7	0.0
		Ave.	7.2	13.7	21	22.6	17.3	11.2	5.3	1.8	0
	L2P2	1	15.5	29.4	29.7	18.4	5.5	1.4	0.1	0.0	0.0
		2	21.1	30.5	30.0	13.0	4.2	0.9	0.3	0.0	0.0
		3	15.9	30.0	31.1	15.2	5.6	1.3	0.7	0.1	0.0
		Ave.	17.8	29.8	29.8	15.6	5.1	1.4	0.4	0.2	0
	L3P2	1	17.9	28.2	29.5	16.9	5.6	1.6	0.2	0.0	0.0
		2	13.0	29.9	31.5	17.9	6.4	1.0	0.2	0.0	0.0
		3	17.2	27.1	27.7	18.8	5.8	1.7	0.8	0.6	0.2
		Ave.	16.1	28.4	29.7	17.9	5.9	1.4	0.4	0.2	0.1
	L4P2	1	18.6	29.7	25.4	17.4	5.9	1.7	0.8	0.4	0.0
		2	16.1	28.8	35.2	12.7	5.5	0.8	0.8	0.0	0.0
		3	21.3	29.4	21.7	16.6	7.7	1.7	0.9	0.0	0.9
		Ave.	18.6	29.3	27.6	15.5	6.3	1.4	0.8	0.1	0.3

Table 15. Fatigue damage of PTO shaft according to operating conditions.

Operating conditions		Tillage pitch (cm)	Fatigue damage			
			1	2	3	Average
Site 1	L2P1	0.82	1.68×10^{-8}	1.7×10^{-8}	1.35×10^{-8}	1.58×10^{-8}
	L3P1	1.18	1.94×10^{-8}	2.14×10^{-8}	1.47×10^{-8}	1.85×10^{-8}
	L4P1	1.57	1.11×10^{-8}	4.89×10^{-8}	2.91×10^{-8}	2.97×10^{-8}
	L2P2	0.62	4.4×10^{-9}	1.15×10^{-8}	5.49×10^{-9}	7.13×10^{-9}
	L3P2	0.89	8.91×10^{-9}	5.09×10^{-9}	1.09×10^{-8}	8.30×10^{-9}
	L4P2	1.19	6.95×10^{-9}	1.12×10^{-8}	1.03×10^{-8}	9.48×10^{-9}
Site 2	L2P1	0.83	2.3×10^{-8}	3×10^{-8}	3.05×10^{-8}	2.78×10^{-8}
	L3P1	1.20	3.27×10^{-8}	4.27×10^{-8}	2.25×10^{-8}	3.26×10^{-8}
	L4P1	1.61	4.86×10^{-8}	3.63×10^{-8}	3.36×10^{-8}	3.95×10^{-8}
	L2P2	0.63	9.25×10^{-9}	6.37×10^{-9}	1.34×10^{-8}	9.67×10^{-9}
	L3P2	0.90	8.14×10^{-9}	8.63×10^{-9}	1.48×10^{-8}	1.05×10^{-8}
	L4P2	1.21	1.18×10^{-8}	8.39×10^{-9}	1.94×10^{-8}	1.32×10^{-8}

PTO shaft, tillage pitch, and soil strength. The analysis revealed significant correlations between PTO shaft fatigue damage and the following factors: tractor travel speed ($p<0.10$), power consumed by the PTO shaft ($p<0.05$), rotational speed of the PTO shaft ($p<0.01$), tillage pitch ($p<0.01$), and soil strength ($p<0.05$). The correlation coefficients were ranked in descending order as follows: rotational speed of the PTO shaft > tillage pitch > soil strength > consumed power of the PTO shaft > tractor travel speed. This indicates that the rotational speed of the PTO shaft is the most influential factor affecting fatigue damage. Moreover, the rotational speed and consumed power of the PTO shaft exhibited a negative correlation with fatigue damage, while tillage pitch, soil strength, and tractor travel speed exhibited positive correlations. These findings suggest that increased PTO shaft fatigue damage is associated with lower rotational speed and power of the PTO shaft, as well as higher tillage pitch, soil strength, and tractor travel speed. Notably, the power consumed by the engine did not significantly influence PTO shaft fatigue damage. Regression analysis was conducted using the tractor travel speed, power consumed by the PTO shaft, rotational speed of the PTO shaft, tillage pitch, and soil strength as independent variables. Table 17 presents the independent variables, coefficients of determination, root mean square errors (RMSE), F-values, and p-values for the five prediction formulas derived using the stepwise method. The p-values for all five prediction formulas were less than 0.01, indicating statistical significance. Among these formulas, the No. 5 prediction formula, which incorporated all significant independent variables, achieved the highest coefficient of determination ($R^2 = 0.93$) and the lowest RMSE (2.94×10^{-9}). The regression coefficients for the No. 5 prediction formula are detailed in Table 18, and the final PTO shaft fatigue damage prediction formula is expressed as Eq. 13. Figure 22 illustrates the variance between the PTO shaft fatigue damage

Table 16. Results of Pearson's correlation analysis for damage of PTO shaft.

Item		Actual travel speed	Engine power	PTO power	PTO speed	Tillage pitch	Soil strength
Damage of PTO	Correlation coefficient	0.29*	-0.22	-0.32**	-0.79***	0.65***	0.37**
	p	0.08	0.20	0.05	0.00	0.00	0.03
	N	36	36	36	36	36	36

p*<0.10, p**<0.05, p***<0.01.

Table 17. Results of stepwise regression analysis for PTO shaft fatigue damage.

No. of prediction formula	Independent variable	Coefficient of determination (R^2)	Root mean square error (RMSE)	F-value	p
1	PTO speed	0.62	6.98×10-9	55.38	0.00
2	PTO speed Soil strength	0.84	4.59×10-9	83.63	0.00
3	PTO speed Soil strength Tillage pitch	0.91	3.37×10-9	109.64	0.00
4	PTO speed Soil strength Tillage pitch Actual travel speed	0.92	3.20×10-9	89.12	0.00
5	PTO speed Soil strength Tillage pitch Actual travel speed PTO power	0.93	2.94×10-9	83.17	0.00

Table 18. Regression coefficient for prediction formula No. 5 in Table 17.

Dependent variable	Independent variable	Standardization regression coefficient (B)	Standard error (S.E)	Standardized coefficients (β)	t-value	p
Fatigue damage of PTO shaft	Constant	1.26×10^{-8}	0.000	-	0.856	0.399
	PTO speed	-4.88×10^{-11}	0.000	-0.396	-2.153	0.040
	Soil strength	1.75×10^{-11}	0.000	0.392	7.520	0.000
	Tillage pitch	4.57×10^{-8}	0.000	1.267	3.282	0.003
	Actual travel speed	-1.66×10^{-8}	0.000	-0.917	-2.646	0.013
	PTO power	5.38×10^{-10}	0.000	0.216	2.381	0.024

predicted by the No. 5 formula and the actual measured values:

$$D_{PTO} = (-4.88 \times N_{PTO} + 1.75 \times CI + 4573.11 \times T_P - 1658.64 \times V_{act} + 53.84 \times P_{PTO} + 1262.94) \times 10^{-11}$$

(Eq. 13)

where: D_{PTO} = fatigue damage of PTO shaft; N_{PTO} = rotational speed of PTO shaft (rpm); C_I = cone index (soil strength) (kPa); T_P = tillage pitch (cm); V_{act} = actual travel speed of tractor (km h^{-1}); P_{PTO} = consumed power of PTO shaft (kW).

Conclusions

In this study, PTO shaft fatigue damage during rotary tillage was analyzed under various operating conditions, including soil strength, and a predictive equation for fatigue damage was developed through regression analysis. Rotary tillage was conducted using a rotavator attached to a 42-kW class tractor on two different soil types in Sinbuk-eup, Chuncheon-si, Gangwon-do, Korea. Torque and rotational speed of the engine and PTO shaft, tractor travel speed, and soil strength were measured at multiple locations, and fatigue damage was calculated based on the measured torque data of the PTO shaft.

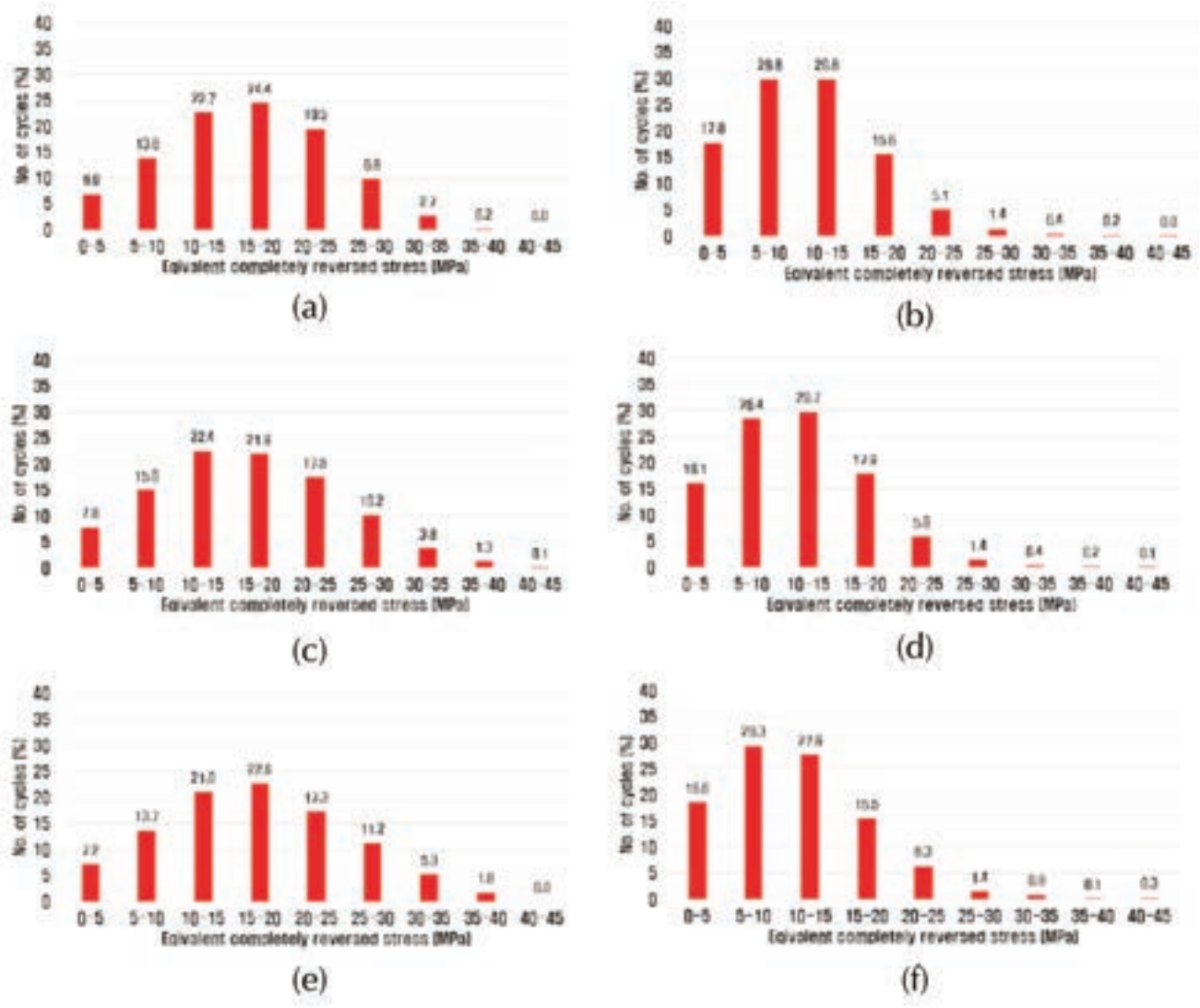

Figure 18. Percentage of equivalent completely reversed shear stress according to operating conditions at site 2. **a**) L2P1; **b**) L2P2; **c**) L3P1; **d**) L3P2; **e**) L4P1; **f**) L4P2.

The analysis revealed that PTO shaft fatigue damage increased with higher transmission gear stages and lower PTO gear stages, attributed to the increased frequency of relatively high equivalent completely reversed stresses under these conditions. Additionally, higher soil strength contributed to greater fatigue damage. To enhance PTO shaft fatigue life, it is recommended to perform rotary tillage with reduced transmission gear stages and increased PTO gear stages within appropriate operating ranges.

Pearson's correlation analysis underscored the significant influence of tractor travel speed, consumed power of the PTO shaft, rotational speed of the PTO shaft, tillage pitch, and soil strength on PTO shaft fatigue damage. Among these, the rotational speed of the PTO shaft was identified as the most influential factor, exhibiting a negative correlation with fatigue damage alongside the power consumed by the PTO shaft. Conversely, tillage pitch, soil strength, and tractor travel speed exhibited positive correlations. Using the stepwise regression analysis method, a predictive equation for PTO shaft fatigue damage was developed. This equation, which incorporates all significant variables affecting fatigue damage, demonstrated high accuracy with a coefficient of determi-

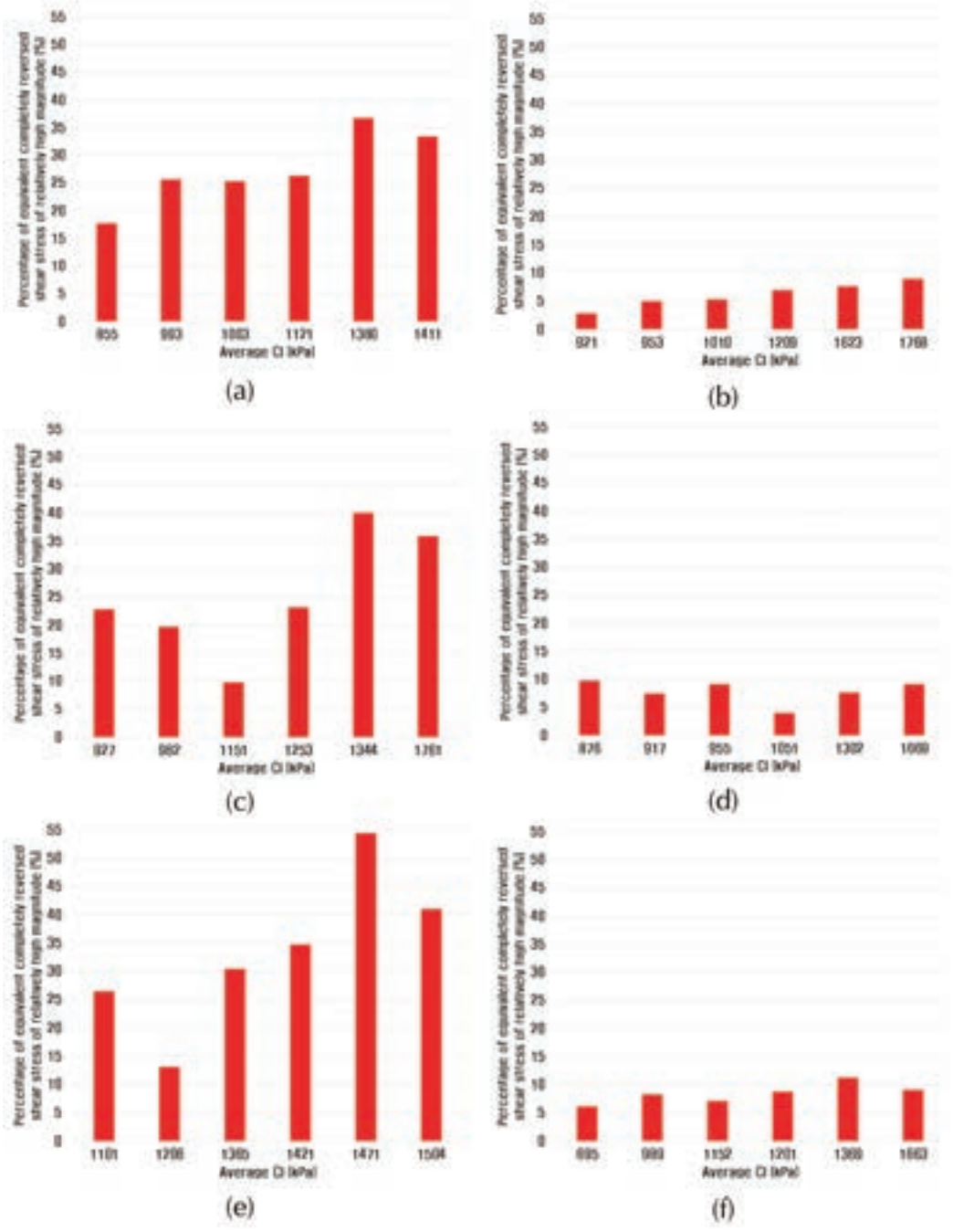

Figure 19. Percentage of equivalent completely revered shear stress of 20 MPa or more according to average CI. **a**) L2P1; **b**) L2P2; **c**) L3P1; **d**) L3P2; **e**) L4P1; **f**) L4P2.

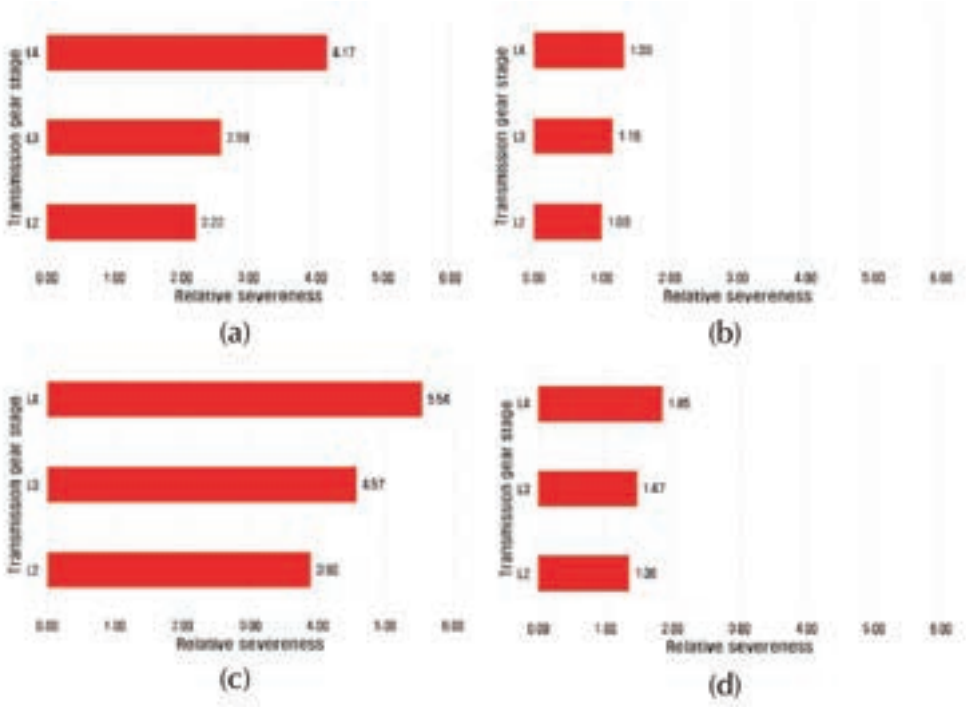

Figure 20. Relative severeness according to transmission and PTO gear stages. **a**) Site 1 - PTO gear 1; **b**) Site 1 - PTO gear 2; **c**) Site 2 - PTO gear 1; **d**) Site 2 - PTO gear 2.

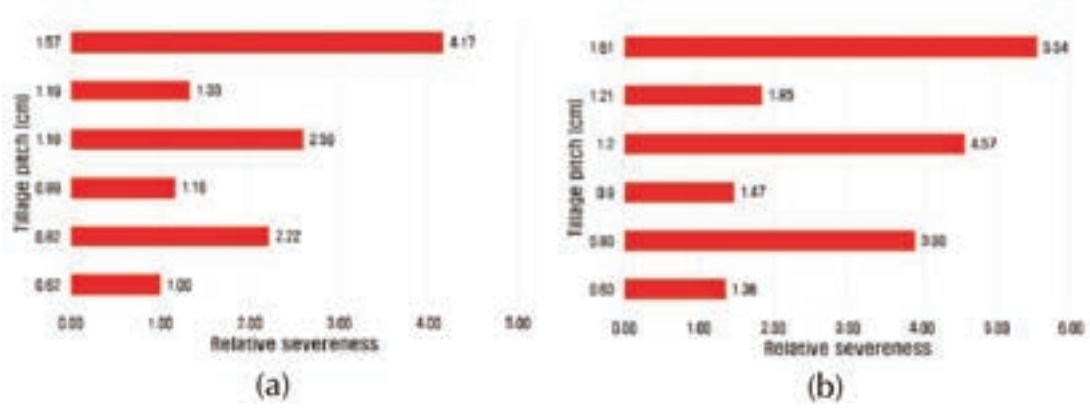

Figure 21. Relative severeness according to tillage pitch. **a**) Site 1; **b**) Site 2.

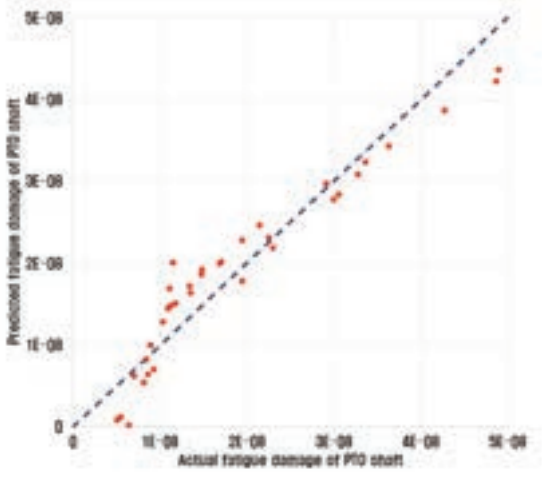

Figure 22. Comparison of predicted and measured PTO shaft fatigue damage.

nation ($R^2 = 0.93$) and a root mean square error (RMSE = 2.94×10^{-9}). The predictive equation provides a valuable tool for identifying PTO shaft fatigue damage tendencies under varying operating conditions.

References

Al-Dosary, N.M.N., Aboukarima, A.M., Al-Hamed, S.A., 2022. Evaluation of artificial neural network to model performance attributes of a mechanization unit (tractor-chisel plow) under different working variables. Agriculture (Basel) 12:840.

Amzallag, C., Gerey, J.P., Robert, J.L., Bahuaud, J., 1994. Standardization of the rainflow counting method for fatigue analysis. Int. J. Fatigue. 16:287-293.

Anthes, R.J., 1997. Modified rainflow counting keeping the load sequence. Int. J. Fatigue. 19:529-35.

Asare, E., Segarra, E., 2018. Adoption and extent of adoption of georeferenced grid soil sampling technology by cotton producers in the southern US. Precision Agric. 19:992-1010.

Baek, S.M., Kim, W.S., Park, S.U., Kim, Y.J., 2019. Analysis of equivalent torque of 78-kW agricultural tractor during rotary tillage. J. Korea Inst. Inf. Electron. Commun. Technol. 12:359-65.

Blanchet, F.G., Legendre, P., Borcard, D., 2008. Forward selection of explanatory variables. Ecology 89:2623-32.

Chai, T., Draxler, R.R., 2014. Root mean square error (RMSE) or mean absolute error (MAE)? – Arguments against avoiding RMSE in the literature. Geosci. Model Dev. 7:1247-50.

Grubisic, V., 1994. Determination of load spectra for design and testing. Int. J. Veh. Des. 15:8-26.

Hensh, S., Tewari, V.K., Upadhyay, G., 2021. An instrumentation system to measure the loads acting on the tractor PTO bearing during rotary tillage. J. Terramech. 96:1-10.

Hodson, T.O., 2022. Root-mean-square error (RMSE) or mean absolute error (MAE): When to use them or not. Geosci. Model Dev. 15:5481-7.

Hwang, S.J., Kim, J.H., Jang, M.K., Nam, J.S., 2022. Correlation between tractor variables and loan support limit in South Korea through regression analysis. J. Biosyst. Eng. 47:402-8.

Hwang, S.J., Kim, J.H., Jang, M.K., Nam, J.S., 2022. Prediction model of loan support limit of plows and rotavators used in South Korea by regression analysis. J. Biosyst. Eng. 47:409-16.

Jabro, J.D., Stevens, W.B., Iversen, W.M., Sainju, U.M., Allen, B.L., 2021. Soil cone index and bulk density of a sandy loam under no-till and conventional tillage in a corn-soybean rotation. Soil Till. Res. 206:104842.

Kamal, M., Rahman, M.M., 2018. Advances in fatigue life modeling: A review. Renew. Sustain. Energy Rev. 82:940-9.

Karunasingha, D.S.K., 2022. Root mean square error or mean absolute error? Use their ratio as well. Inf. Sci. 585:609-29.

Kerry, R., Oliver, M.A., 2004. Average variograms to guide soil sampling. Int. J. Appl. Earth Obs. Geoinf. 5:307-25.

Kim, D.C., Nam, J.S., Kim, M.H., Choe, J.S., Inoue, E., Okayasu, T., Kim, D.C., 2013a. Analysis of the tillage and power consumption characteristics of a crank–type rotavator according to the tillage blade shape. J. Fac. Agric. Kyushu Univ. 58:319-28.

Kim, J.G., Kim, Y.J., Kim, J.H., Shin, B.S., Nam, J.S., 2018. Consumed-power and load characteristics of a tillage operation in an upland field in Republic of Korea. J. Biosyst. Eng. 43:83-93.

Kim, J.G., Park, J.S., Choi, K.J., Lee, D.K., Shin, M.S., Oh, J.Y., Nam, J.S., 2020. Analysis of agricultural tractor transmission using actual farm workload. J. Korean Soc. Manuf. Process Eng. 19:42-48.

Kim, M.H., Nam, J.S., Kim, D.C., 2013b. Comparison of tillage and loads characteristics of three types of rotavators: Rotary-type, crank-type, and plow-type. Biosyst. Eng. 38:73-80.

Kim, S.J., Gim, D.H., Jang, M.K., Hwang, S.J., Kim, J.H., Yang, Y.J., Nam, J.S., 2023. Development of regression model for predicting the maximum static friction force of tractors with a front-end loader. J. Biosyst. Eng. 48:329-38.

Kim, S.S., Lee, Y.S., Woo, J.K., 1997. Tilling load characteristic analysis according to the shape factors of rotary blade. Biosyst. Eng. 06c:18-24.

Kim, W.S., Kim, Y.J., Baek, S.M., Beak, S.Y., Moon, S.P., Lee, N.G., et al 2020. Effect of the cone index on the work load of the agricultural tractor. J. Drive Control. 17:9-18.

Kim, W.S., Kim, Y.J., Park, S.U., Hong, S.J., Kim, Y.S., 2019. Evaluation of PTO severeness for 78-kW-class tractor according to disk plow tillage and rotary tillage. J. Drive Control. 16:23-31.

Kim, Y.J., Chung, S.O., Choi, C.H., Lee, D.H., 2011. Evaluation of tractor PTO severeness during rotary tillage operation. Biosyst. Eng. 36:163-70.

Kim, Y.S., Bae, B.M., Kim, W.S., Kim, Y.J., Lee, S.D., Kim, T.J., 2023. Working load analysis of a 42 kW class agricultural tractor according to tillage type and gear selection during rotary tillage operation. Agriculture (Basel) 13:1556.

Kim, Y.S., Kim, W.S., Baek, S.Y., Baek, S.M., Kim, Y.J., Lee, S.D., Kim, Y.J., 2020. Analysis of tillage depth and gear selection for mechanical load and fuel efficiency of an agricultural tractor using an agricultural field measuring system. Sensors (Basel). 20:2450.

Kumar, A., Chen, Y., Sadek, M.A.A., Rahman, S., 2012. Soil cone index in relation to soil texture, moisture content, and bulk density for no-tillage and conventional tillage. Agric. Eng. Int. CIGR J. 14:26-37.

Kumari, A., Raheman, H., 2023. Tillage operation with a tractor drawn rotavator using an embedded advisory system for minimizing fuel consumption. J. Biosyst. Eng. 48:487-502.

Lee, D.H., Kim, Y.J., Chung, S.O., Choi, C.H., Lee, K.H., Shin, B.S., 2015. Analysis of the PTO load of a 75kW agricultural tractor during rotary tillage and baler operation in Korean upland fields. J. Terramech. 60:75-83.

Lee, W.S., Lee, H.W., 1998. A study on the prediction of the fatigue life of a lug through the finite element analysis. J. Korean Soc. Precis. Eng. 15:88-95.

Lee, Y.S., Lee, J.H., Kwon, Y.N., Ishikawa, T., 2004. Effects of material properties on elastic characteristics of cold forged part. Mater. Sci. Forum. 449-52: 853-6.

Libin, Z., Jiandong, J., Yanbiao, L., 2010. Agricultural rotavator power requirement optimization using multi-objective probability parameter optimization. Int. Agric. Eng. J. 19:15-22.

Mallarino, A.P., Wittry, D.J., 2004. Efficacy of grid and zone soil sampling approaches for site-specific assessment of phosphorus, potassium, pH, and organic matter. Precis. Agric. 5:131-44.

Myung, B.S., Lee, H.D., 2009. Research on the actual condition of rotary tilling & rotary power requirement in the central area. J. Korean Soc. Ind. Converg. 12:79-83.

Naderloo, L., Alimadani, R., Akram, A., Javadikia, P., Khanghah, H.Z., 2009. Tillage depth and forward speed effects on draft of three primary tillage implements in clay loam soil. J. Food Agric. Environ. 7:382-5.

Nam, J.S., Kim, D.C., Kim, M.H., Kim, D.C., 2012. Tillage characteristics estimation of crank-type and rotary-type rotavators by motion analysis of tillage blades. Biosyst. Eng. 37:279-286.

Natpukkana, P., Pakinsee, S., Boonmapat, S., Mitsomwang, P., Borrisutthekul, R., Panuwannakorn, R., Khoa-Phong, L., 2018. Investigation of notch shear cutting for JIS SCM420 steel wire rod. IOP Conf. Ser. Mater. Sci. Eng. 436:012013.

Park, S.H., Lee, D.H., Kim, H.J., Lee, C.S., Cho, S.C., Kwak, T.Y., 2002. Development of dry paddy seeder of strip tillage. Biosyst. Eng. 27:25-32.

Rousson, V., Goşoniu, N.F., 2007. An -square coefficient based on final prediction error. Stat. Methodol. 4:331-340.

Ryu, M.J., Chung, S.O., Kim, Y.J., Lee, D.H., Choi, C.H., Lee, K.H., 2012. FFT analysis of load data during field operations using a 75-kW agricultural tractor. Korean J. Agric. Sci. 40:53-59.

Ryu, M.J., Kang, S.W., Chung, S.O., Kim, Y.J., Lee, D.H., Choi, C.H., 2013. Load characteristics of 30 and 75-kW agricultural tractors during field operations. Proc. American Society of Agricultural and Biological Engineers, Kansas City, July 21-24, paper number 131590237,

Santecchia, E., Hamouda, A.M.S., Musharavati, F., Zalnezhad, E., Cabibbo, M., El Mehtedi, M., Spigarelli, S., 2016. A review on fatigue life prediction methods for metals. Adv. Mater. Sci. Eng. 2016:1-26.

Shigley, J.E., Budynas, R.G., Nisbett, J.K., 2020. Mechanical engineering design. 11th ed. McGraw-Hill, p. 212-256.

ASABE Standard S313.3, 2018. Soil cone penetrometer. St. Joseph, American Society of Agricultural and Biological Engineers.

ASABE Standard EP542.1, 2019. Procedures for using and reporting data obtained with the soil cone penetrometer. St. Joseph, American Society of Agricultural and Biological Engineers.

Sutter, J.M., Kalivas, J.H., 1993. Comparison of forward selection, backward elimination, and generalized simulated annealing for variable selection. Microchem. J. 47:60-6.

Tan, K.H., 2005. Soil sampling, preparation, and analysis. Boca Raton, CRC Press.

Thompson, B., 1995. Stepwise regression and stepwise discriminant analysis need not apply here: A guidelines editorial. Educ. Psychol. Meas. 55:525-34.

Wollenhaupt, N.C., Wolkowski, R.P., 1994. Grid soil sampling. Better Crops 78:6-9.

Yadav, R.K., Singh, P., Singh, S.K., 2017. Performance analysis of rotavator and other tillage implement driven by the tractor. Int. J. Agric. Eng. 10:590-4.